Interactive Crop Management in the Community Earth System Model (CESM1): Seasonal Influences on Land–Atmosphere Fluxes

SAMUEL LEVIS, GORDON B. BONAN, AND ERIK KLUZEK

National Center for Atmospheric Research, Boulder, Colorado

PETER E. THORNTON

Oak Ridge National Laboratory, Oak Ridge, Tennessee

ANDREW JONES

Lawrence Berkeley National Laboratory, Berkeley, California

WILLIAM J. SACKS

National Center for Atmospheric Research, Boulder, Colorado

CHRISTOPHER J. KUCHARIK

University of Wisconsin—Madison, Madison, Wisconsin

ABSTRACT

The Community Earth System Model, version 1 (CESM1) is evaluated with two coupled atmosphere–land simulations. The CTRL (control) simulation represents crops as unmanaged grasses, while CROP represents a crop managed simulation that includes special algorithms for midlatitude corn, soybean, and cereal phenology and carbon allocation. CROP has a more realistic leaf area index (LAI) for crops than CTRL. CROP reduces winter LAI and represents the spring planting and fall harvest explicitly. At the peak of the growing season, CROP simulates higher crop LAI. These changes generally reduce the latent heat flux but not around peak LAI (late spring/early summer). In midwestern North America, where corn, soybean, and cereal abundance is high, simulated peak summer precipitation declines and agrees better with observations, particularly when crops emerge late as is found from a late planting sensitivity simulation (LateP). Differences between the CROP and LateP simulations underscore the importance of simulating crop planting and harvest dates correctly. On the biogeochemistry side, the annual cycle of net ecosystem exchange (NEE) also improves in CROP relative to Ameriflux site observations. For a global perspective, the authors diagnose annual cycles of CO_2 from the simulated NEE (CO_2 is not prognostic in these simulations) and compare against representative GLOBALVIEW monitoring stations. The authors find an increased (thus also improved) amplitude of the annual cycle in CROP. These regional and global-scale refinements from improvements in the simulated plant phenology have promising implications for the development of the CESM and particularly for simulations with prognostic atmospheric CO_2.

1. Introduction

Past studies indicate that managed and unmanaged terrestrial ecosystems interact with the atmosphere and Other components of the earth system through a variety of biogeophysical and biogeochemical processes and characteristics. Levis (2010) reviews this topic. In the present study we consider such effects by simulating certain managed ecosystems.

Managed ecosystems add to simulations of the earth system the uncertainty of human interference. Numerous climate-modeling studies have explored the effects of

Corresponding author address: Samuel Levis, National Center for Atmospheric Research, P.O. Box 3000, Boulder, CO 80307-3000.
E-mail: slevis@ucar.edu

human land use on the earth system by usually replacing trees in land surface models with a simplistic representation of crops, such as grasses (Pitman et al. 2009). However, realistic crop phenology and the use of fertilizer and irrigation give croplands different biogeophysical and biogeochemical characteristics relative to grasslands.

Xue et al. (1996) reduced North American temperature biases in their coupled land–atmosphere model by prescribing more appropriate values of certain vegetation parameters to their crops. A few years later, climate modelers began introducing adaptations of complex crop models into land surface models to better depict managed ecosystems (Tsvetsinskaya et al. 2001a), as they had done earlier with ecosystem models of unmanaged vegetation (Foley et al. 1996). Originally intended to facilitate agricultural management, such crop models usually combine mechanistic and empirical algorithms to simulate complex crop behavior to project yields for a range of nutrient and water availabilities and weather conditions at local to regional scales (e.g., Hodges et al. 1987).

Climate scientists first used crop models to simulate the effects of climate change on crops (e.g., Mearns et al. 1999). Such studies neglected potential two-way climate–crop interactions, so Tsvetsinskaya et al. (2001a,b) coupled a regional climate model to a crop model in a proof-of-concept exploration of climate–crop interactions over the central Great Plains of North America. Tsvetsinskaya et al. found that replacing the regional climate model's generic crop formulation with the more realistic representation of corn from a crop model led to improvements in the simulated leaf area index (LAI). These improvements generated differences in the simulated turbulent heat fluxes, which led to changes in temperature, humidity, winds, and precipitation. At interannual time scales the largest changes were found during drought years and at diurnal time scales during the midafternoon. With the more realistic representation of corn, the precipitation was simulated closer to the observed.

Soon many others (Kucharik and Brye 2003; Bondeau et al. 2007; Osborne et al. 2007; Stehfest et al. 2007; Gervois et al. 2008; Levis et al. 2009; Lokupitiya et al. 2009) adapted their land surface models to include realistic crop algorithms for eventual use in comprehensive earth system models. The goal was to simulate fundamental drivers of crop management and growth dynamics interactively rather than using datasets that may not hold under future climate conditions. Most studies using such models have explored a variety of agricultural issues without coupling to atmospheric models. For example, Twine et al. (2004) used the Agro-IBIS (Integrated BIosphere Simulator) model to investigate the biogeophysical effects of replacing an undisturbed Wisconsin grassland or forest with crops. From grassland to crop, which is the case pertinent to our study, they found increased net radiation and evapotranspiration, mainly in response to reduced surface albedo. Again, such studies do not account for possible two-way climate–crop interactions.

Only Osborne et al. (2007, 2009) performed *global coupled* atmosphere–land simulations with an interactive crop model. Osborne et al. used the crop model GLAM (a groundnut, i.e., warm climate crop, model) in the land component of the Hadley Centre Atmosphere Model, version 3 (HadAM3). Osborne et al. (2009) examined the effect of interactive, as opposed to prescribed, crop phenology on tropical climate variability and found increased growing season variability in evapotranspiration, relative humidity, and temperature.

In the present study, we replace the Community Land Model's (CLM's) unmanaged "grass-like" crop with managed corn, soybean, and temperate cereals as in Agro-IBIS (Kucharik and Brye 2003). We take this opportunity to document the CLM crop model as part of the special collection of articles documenting the Community Earth System Model, version 1 (CESM1) in the *Journal of Climate.* Furthermore, we examine changes in the interactions simulated by our global coupled land–atmosphere model by introducing the interactive crop management model. As in Tsvetsinskaya et al. (2001a), we test the null hypothesis that replacing unmanaged with managed crops does not affect our model's simulated climate.

Osborne et al. (2009) focused on tropical regions, while we focus on the midlatitudes and especially midwestern North America, where corn, soybean, and temperate cereals exist in higher concentrations than elsewhere. Past work has identified sensitive regions of potentially strong land–atmosphere coupling in North America (e.g., Koster et al. 2004). We do not address physical climate effects from crops on the global scale or in remote regions through teleconnections.

From midwestern North America to the global scale we do evaluate the model's simulation of carbon fluxes. Lokupitiya et al. (2009) found that using a crop model to represent crops in a land surface model led to better simulated LAI and that this resulted in better simulated carbon fluxes at the land–atmosphere interface in the central United States. Better simulated carbon fluxes will likely improve earth system model simulations with prognostic atmospheric CO_2 concentrations.

2. Methods

a. Model description

We perform coupled simulations with the Community Atmosphere Model, version 4 (CAM4.0) (Neale et al. 2012, manuscript submitted to *J. Climate*) and the Community Land Model with Carbon and Nitrogen

(CLM4CN) biogeochemistry (Lawrence et al. 2012). These are component models of CESM1 (available online at http://www.cesm.ucar.edu). We prescribe climatological sea ice and sea surface temperatures (SSTs) (Neale et al. 2012, manuscript submitted to *J. Climate*) to eliminate interannual atmospheric variability due to coupled ocean–atmosphere interactions. References in this paragraph include extensive model documentation and evaluation and appear with this article in the *Journal of Climate* special collections dedicated to the CESM1 and Community Climate System Model, version 4 (CCSM4).

Here we document the crop-specific phenology and carbon allocation algorithms added to the unmanaged vegetation framework of the CLM4CN (Lawrence et al. 2012). These crop algorithms originate in Agro-IBIS, another state-of-the-art land surface model with similar options to simulate dynamic vegetation (Kucharik et al. 2000) and interactive crop management (Kucharik and Brye 2003). Agro-IBIS was evaluated favorably for agricultural sites and regions in the North American midlatitudes (Kucharik 2003; Donner and Kucharik 2003; Kucharik and Twine 2007; Twine and Kucharik 2008). In the CLM, the crop algorithms were first tested in offline simulations with CLM3.5CN (Levis et al. 2009). These algorithms have now been released as an optional configuration to the CLM user community with instructions in the corresponding user's guide (Kluzek 2011).

The crop algorithms use temperature to drive growing-season transitions in phenology and carbon allocation. Generally speaking, carbon allocation to crop leaf, fine root, live stem, and reproductive pools begins with leaf emergence and ends at harvest. However, as an example of a growing season transition, allocation to the reproductive pool occurs only during the last phase of crop development, identified as the phase from grain fill to physiological maturity and harvest.

The CLM plant functional types (pfts) include an unmanaged crop, modeled like an unmanaged C3 grass and distributed spatially according to satellite data (Oleson et al. 2010).[1] Here we introduce three new pfts—corn (CLM's only C4 crop), soybean, and temperate cereals—with gridcell coverage from the 1992 crop dataset of Ramankutty and Foley (1998) (Fig. 1a). We change several pft parameter values following Agro-IBIS, to further distinguish corn, soybean, and temperate cereals from the unmanaged crop. In many—usually warmer—areas, farmers plant cereals, such as winter wheat, in the fall for a late spring harvest. Here we do not represent winter cereals and treat all our temperate cereals as warm season crops, like spring wheat, owing to the unavailability of global data that distinguish winter from spring cereals. Furthermore, we define temperate cereals as the sum of wheat, barley, and rye, assuming that these three crops have very similar characteristics and could be treated as one plant functional type, following Table 1 of Bondeau et al. (2007). We assign to wheat, barley, and rye the pft definitions for wheat.

To allow managed and unmanaged vegetation to coexist in a model grid cell and be handled separately by CLM's crop and dynamic vegetation models, we divide the CLM vegetated land unit in two parts. Pfts in the unmanaged land unit all share the same below-ground properties per grid cell, including water and nutrients (CLM4CN default option, Fig. 1b). Pfts in the managed land unit occupy separate soil columns, that is, they do not interact with each other below the ground and, therefore, do not compete for water and nutrients (Fig. 1c). This permits different management practices, such as irrigation and fertilization, per crop. Implementations of prognostic irrigation (Levis and Sacks 2011) and fertilization (B. Drewniak 2011, personal communication) are forthcoming. Until then, we consider all pfts as rainfed, and we disable the CLM4CN interactive nitrogen limitation for corn, soybean, and temperate cereals. For these three pfts we prescribe the V_{cmax25} value proposed for crops (101 μmol CO_2 m^{-2} s^{-1}) by Kattge et al. (2009) as in Bonan et al. (2011).

CLM4CN calculates the LAI as a function of each pft's leaf carbon and specific leaf area. A detailed technical description of this crop model appears in the appendix.

b. *The simulations*

We perform three 41-yr equilibrium present-day CAM4–CLM4CN simulations at 1.9° latitude by 2.5° longitude resolution with all of the default model settings and inputs associated with this resolution (Gent et al. 2011). We average results from the last 20 years of each simulation.

1) CTRL, the control simulation, which represents crops as unmanaged C3 grasses and applies nitrogen limitation to all pfts as in the default CLM4CN.
2) CROP, the selectively managed simulation, which includes phenology and carbon allocation algorithms specific to midlatitude corn, soybeans, and temperate cereals. In grid cells where the managed crops sum to less than the CLM total crop fractional cover, we continue to employ the unmanaged crop pft for the remaining portion. Because our model is specific to midlatitude crops, we restrict our implementation to regions above 30° in the Northern and Southern Hemispheres and retain the unmanaged crop pft in the tropics.
3) LateP, the late planting simulation, in which the managed crops are planted on the latest date allowed

[1] C3 and C4 refer to different photosynthetic pathways of plants.

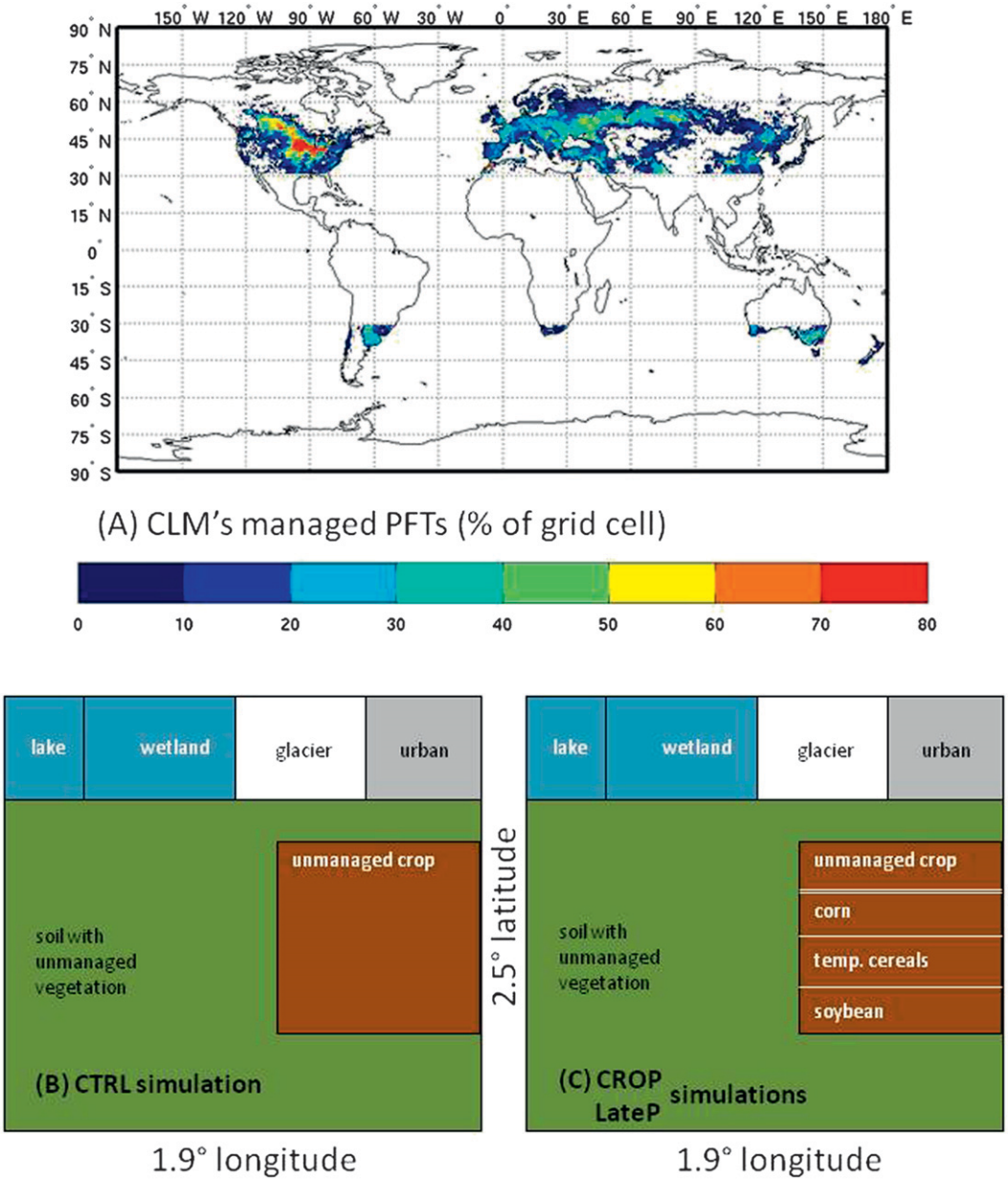

FIG. 1. (a) Percent cover of the sum of managed crop plant functional types (pfts) in the CLM based on the data of Ramankutty and Foley (1998). Managed crop pfts in the CLM are corn, soybean, and temperate cereals. Crop area in the zone 30°S–30°N is assigned to the unmanaged crop pft. (b) Schematic of a CLM grid cell, its land units, and crop pfts in the CTRL simulation vs (c) in the CROP and LateP simulations.

by the model (see section b of the appendix). We investigate whether differences in the resulting growing seasons simulated by LateP and CROP influence the atmospheric state.

c. *Data for model evaluation*

We compare the simulated precipitation (P) and temperature (T_{2m}) in midwestern North America to data from Willmott and Matsuura (2000). Here we define midwestern North America as the contiguous region in the world where corn, soybean, and temperate cereals sum to more than 52.5% of gridcell cover at 1.9° × 2.5° horizontal spatial resolution. This region has the highest crop cover in the world (Table 1).

We also compare the global simulations at individual grid cells against site observations at two Ameriflux sites. Gap-filled Ameriflux "level 4" data for the rainfed sites in Bondville, Illinois, at 40°N, 88°W (Meyers and

TABLE 1. Cover (%) prescribed from data (sources discussed in the text) per plant functional type over the soil-covered areas of CLM4 grid cells. Selected sites and regions are discussed in the text. Note: where cover does not sum to 100%, the remainder goes to bare ground.

Type	Europe (45°–55°N, 0°–30°E)	Central Russia (52°–56°N, 60°–85°E)	North American Midwest	Mead (41°N, 96°W)	Bondville (40°N, 88°W)
Tree	37	18	6	2	9
Shrub	1	1	0	0	0
Grass	21	37	18	18	23
Unmanaged crop	15	4	9	10	1
Managed crop	23	30	61	66	63

Hollinger 2004) and Mead, Nebraska, at 41°N, 96°W (Verma et al. 2005) include surface heat and CO_2 fluxes, *P*, LAI, and other variables (available online at http://public.ornl.gov/ameriflux/site-select.cfm). Both sites employ no-till agriculture to grow corn and soybean in annual rotation. For Bondville the data span 1996–2006 (except the LAI, which spans 1997–2001) but the year 2000 and the first half of 1996 are missing. For Mead the data span 2001–05 but the first few months of 2001 and the last few months of 2005 are missing. In Mead the LAI data span 2001–08. These time periods are short relative to the 20-yr averages calculated from our simulations. However, representative LAI values tend to emerge even from a small number of years. Hence we emphasize the comparisons of LAI more than of the heat fluxes.

Another source of uncertainty when comparing tower-measured versus model-simulated heat fluxes stems from the spatial scale mismatch between model grid cells (about 200 km) and tower-site footprints (at most a few kilometers) (Randerson et al. 2009). Here, we have not employed upscaling of the tower-site observations (Jung et al. 2009). Instead, we have followed the direct comparison approach of Randerson et al. (2009), who acknowledge low uncertainty in measured surface heat fluxes and net ecosystem exchange (NEE) but moderate to high scaling mismatch with model output. Despite low uncertainty in measured surface heat fluxes, the problem with energy balance closure remains at tower sites (not in models) and suggests that latent plus sensible heat fluxes may be biased low (Wilson et al. 2001).

For a global perspective on the biogeochemical effects of interactive crop management in the CLM4CN, we use the algorithm of Randerson et al. (2009) to diagnose monthly anomalies of CO_2 concentration from the simulated NEE at a subset of GLOBALVIEW network CO_2 monitoring stations (Masarie and Tans 1995). We compare the values from our equilibrium simulations (in this case the last 10 years) against the observed for years 1991–2000.

3. Results

CROP simulates the annual cycle of leaf area index (LAI) for the three managed crops more realistically than for the unmanaged crop plant functional type (pft). In four sample regions (Europe, central Russia, Argentina, and Midwestern North America) the managed crops show reduced winter LAI and clear spring planting and fall harvest periods. At the height of the growing season, the managed crops display higher LAI. In contrast, the unmanaged crop generally displays a flat annual cycle with insufficient seasonal variability (Figs. 2a–d). These differences are statistically significant across a range of sites and regions (Table 2). Some observations show corn LAI exceeding soy LAI (Flénet et al. 1996; Verma et al. 2005), while others show the opposite during certain phases of growth (Thenkabail et al. 2000). Our simulations produce lower corn than soy LAI throughout the growing season. These simulations include no calibration of the CLM4CNcrop model to improve the results of this study in any way.

We evaluate the simulated LAI against observations in Bondville and Mead (Figs. 2e–f). At both sites, the CROP-simulated LAI compares better to the observed than does the CTRL-simulated LAI. At both sites CROP simulates the second half and LateP the first half of the growing season better. Both simulations overestimate the length of the growing season. Both simulations also overestimate the LAI, especially in Mead. The Agro-IBIS developers performed site-specific calibration of the model for Mead, using planting date and hybrid information, and drove the model with meteorological data collected at the site (Kucharik and Twine 2007) to match the observations. We have not performed site-specific calibration of the CLM4CNcrop model.

The phenological changes from the CTRL simulation to CROP and LateP reduce the latent heat flux (L) in fall and winter and usually not in spring and summer. In most regions and seasons shown, the *P* and soil moisture appear reduced, indicating generally drier conditions in response to the inclusion of interactive crop management in the model (Table 2).

Differences between the simulations that we may attribute to the interactive crop management are likely more robust in midwestern North America due to higher managed crop abundance than anywhere else in the

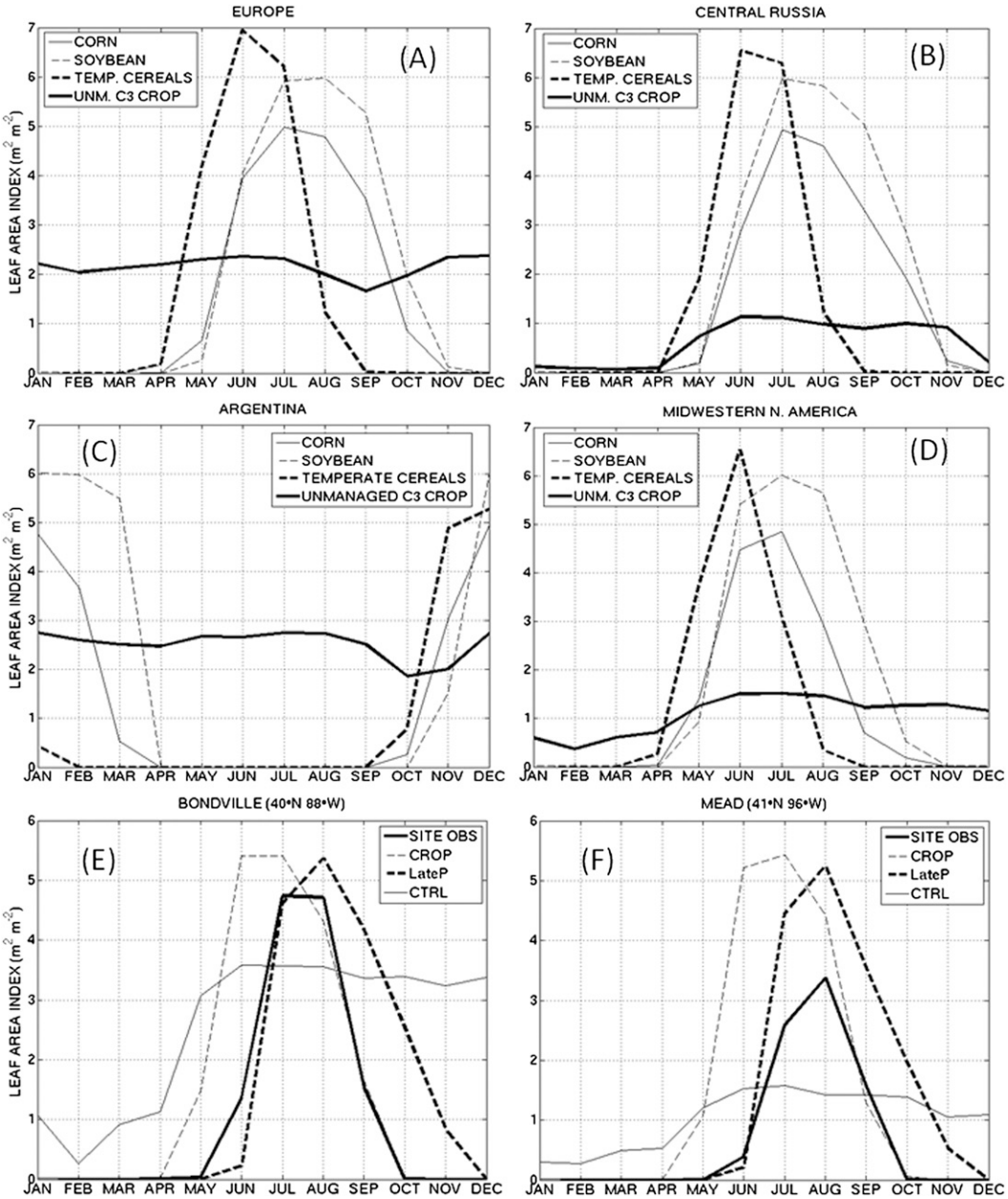

FIG. 2. Twenty-year-average monthly leaf area index (LAI) (m^2 leaf m^{-2} ground) simulated in the CROP simulation. The unmanaged crop behaves similarly in the CTRL simulation (not shown). (a) Europe (45°–55°N, 0°–30°E); (b) central Russia (52°–56°N, 60°–85°E); (c) Argentina as a Southern Hemisphere example (35°–37°S, 59°–61°W); (d) midwestern North America, defined as the contiguous region with managed crop cover exceeding 52.5%; (e) 20-yr average LAI of the unmanaged crop for the CTRL and 20-yr area-weighted average LAI of the corn and soybeans for the CROP and LateP simulations in Bondville, Illinois, vs the site observations (not 20-yr averages, see section 2c); and (f) the same but in Mead, Nebraska. For observed LAIs we average the annually rotating corn and soybean LAIs.

world. Here we find that CROP simulates increased L in May and June relative to the CTRL, while LateP simulates increased L in July and August (Fig. 3a). This pattern is qualitatively similar in Bondville and Mead (Figs. 3b,c). Relative to the observations in Bondville, CROP simulates L better in the second half and LateP in the first half of the growing season, consistent with the simulated versus observed LAI behavior. In Mead the pattern of simulated L is similar, but relative to the observations we can only say that LateP gets closer in

TABLE 2. Key vegetation and climate variables shown as 20-yr averages by region and season for the CTRL simulation; differences are for CROP −CTRL (labeled ΔCROP) and LateP −CTRL (labeled ΔLateP), and boldface indicates statistically significant difference in the means at the 95% confidence level. Variables are LAI: leaf area index, L: latent heat flux, P: precipitation, β: soil moisture limitation on photosynthesis (1 means no limitation), NEE: net ecosystem exchange, α: surface albedo, and R_n: net radiation at the surface; seasons are DJF: December–February, MAM: March–May, and SON: September–November.

LAI (m^2 leaf m^{-2} ground)				L (W m^{-2})			P (mm d^{-1})			β (fraction)			NEE (gC m^{-2} d^{-1})			α (fraction)			R_n (W m^{-2})		
Season	CTRL	ΔCROP	ΔLateP	CTRL	ΔCROP	ΔLateP	CTRL	ΔCROP	ΔLateP	CTRL	ΔCROP	ΔLateP	CTRL	ΔCROP	ΔLateP	CTRL	ΔCROP	ΔLateP	CTRL	ΔCROP	ΔLateP
Europe (45°–55°N, 0°–30°E)																					
DJF	1.95	**−0.47**	**−0.49**	13.1	−0.2	0.0	2.349	−0.049	0.134	0.939	0.013	**0.020**	0.772	**0.276**	**0.314**	0.194	−0.008	−0.007	−5.4	−0.3	−0.3
MAM	2.21	−0.11	**−0.46**	51.5	0.0	**−4.1**	2.504	−0.066	**−0.289**	0.989	**−0.027**	0.002	−0.616	**−0.386**	**0.401**	0.141	0.003	**0.004**	83.7	−0.2	−0.8
JJA	2.71	**0.66**	**0.42**	87.5	−0.2	1.1	1.916	0.086	0.000	0.867	0.007	−0.033	−0.875	**−0.901**	**−1.198**	0.134	**0.007**	**0.005**	143.9	−2.9	0.1
SON	2.32	**−0.40**	**−0.14**	27.1	**−2.0**	**−1.2**	1.933	−0.113	−0.052	0.927	−0.012	**−0.042**	0.483	**0.772**	**0.397**	0.154	0.002	0.001	29.2	−0.8	−0.4
Central Russia (52°–56°N, 60°–85°E)																					
DJF	0.63	**−0.03**	−0.03	1.9	−0.2	−0.3	1.162	0.102	−0.020	0.228	−0.012	0.012	0.325	**0.089**	**0.089**	0.600	**0.026**	−0.006	−19.7	−0.2	−0.3
MAM	0.73	**0.12**	**−0.07**	37.4	2.1	−0.8	1.231	0.046	−0.109	0.686	**−0.047**	0.008	0.012	**−0.176**	**0.451**	0.283	0.012	−0.001	73.9	−1.0	0.5
JJA	1.42	**1.13**	**0.89**	79.4	2.0	3.7	1.883	−0.117	−0.005	0.776	**−0.098**	**−0.079**	−0.588	**−0.972**	**−1.280**	0.162	**0.002**	0.002	137.8	0.7	1.1
SON	1.31	**−0.24**	−0.01	18.4	**−2.7**	−0.5	1.210	−0.001	0.078	0.772	**−0.040**	**−0.034**	0.212	**0.732**	**0.527**	0.215	**0.021**	0.009	13.5	−0.6	0.5
North American Midwest																					
DJF	0.80	**−0.54**	**−0.57**	8.9	**−0.9**	**−1.3**	0.931	−0.059	−0.037	0.528	**−0.041**	−0.024	0.231	**0.310**	**0.349**	0.351	**0.035**	**0.035**	1.9	**−2.4**	**−1.9**
MAM	0.93	**−0.19**	**−0.60**	53.7	0.7	**−6.2**	2.226	−0.006	−0.260	0.874	**−0.057**	0.000	0.318	**−0.513**	**0.906**	0.210	0.004	**0.013**	98.6	0.0	−1.9
JJA	1.83	**1.60**	**0.69**	112.9	0.2	−1.1	3.346	−0.129	**−0.273**	0.801	**−0.130**	**−0.134**	−0.563	**−2.623**	**−2.714**	0.162	**0.004**	**0.009**	162.9	1.6	0.8
SON	1.59	**−0.88**	**−0.32**	36.8	**−7.1**	**−5.0**	1.362	−0.056	0.012	0.760	**−0.044**	**−0.095**	−0.136	**2.164**	**1.088**	0.193	**0.030**	**0.025**	45.0	**−5.2**	**−3.3**
Mead (41°N, 96°W)																					
DJF	0.47	**−0.34**	**−0.35**	8.6	**−1.3**	−0.8	0.557	−0.093	−0.017	0.566	**−0.089**	−0.054	0.207	**0.279**	**0.306**	0.335	0.036	**0.034**	1.6	**−2.7**	**−1.8**
MAM	0.64	−0.07	**−0.48**	48.9	−0.3	**−9.1**	2.011	−0.079	**−0.393**	0.889	**−0.054**	−0.002	0.251	**−0.383**	**0.993**	0.249	0.010	0.023	92.7	−0.1	−3.8
JJA	1.33	**2.04**	**1.09**	115.0	3.0	−1.8	3.598	0.047	−0.178	0.819	**−0.140**	**−0.154**	−0.409	**−3.100**	**−2.986**	0.181	**−0.009**	**0.009**	161.7	**6.2**	1.2
SON	1.11	**−0.60**	0.01	35.4	**−6.9**	−4.5	1.218	−0.057	0.013	0.717	−0.011	−0.056	−0.109	**2.323**	**1.130**	0.213	**0.050**	**0.035**	45.1	**−7.9**	**−4.5**
Bondville (40°N, 88°W)																					
DJF	1.38	**−0.93**	**−1.01**	13.4	−1.1	**−1.8**	1.625	−0.133	−0.172	0.749	−0.003	0.016	0.375	**0.677**	**0.888**	0.236	**0.048**	**0.037**	13.0	**−3.0**	**−2.5**
MAM	1.53	**−0.57**	**−1.04**	69.0	0.8	**−4.6**	3.269	0.100	−0.335	0.991	**−0.080**	0.000	0.821	**−0.511**	**1.276**	0.159	**0.007**	**0.012**	110.9	−1.3	−0.3
JJA	3.32	**0.91**	−0.18	146.7	−2.0	**−7.4**	4.481	**−0.517**	**−0.783**	0.931	−0.035	**−0.102**	−1.003	**−4.497**	**−4.113**	0.132	**0.007**	**0.012**	177.7	1.9	0.1
SON	3.01	**−1.72**	**−0.68**	54.3	**−9.1**	**−4.2**	1.938	−0.085	0.197	0.930	**−0.065**	**−0.062**	−0.496	**3.675**	**1.543**	0.158	**0.018**	**0.012**	61.5	**−6.0**	**−3.0**

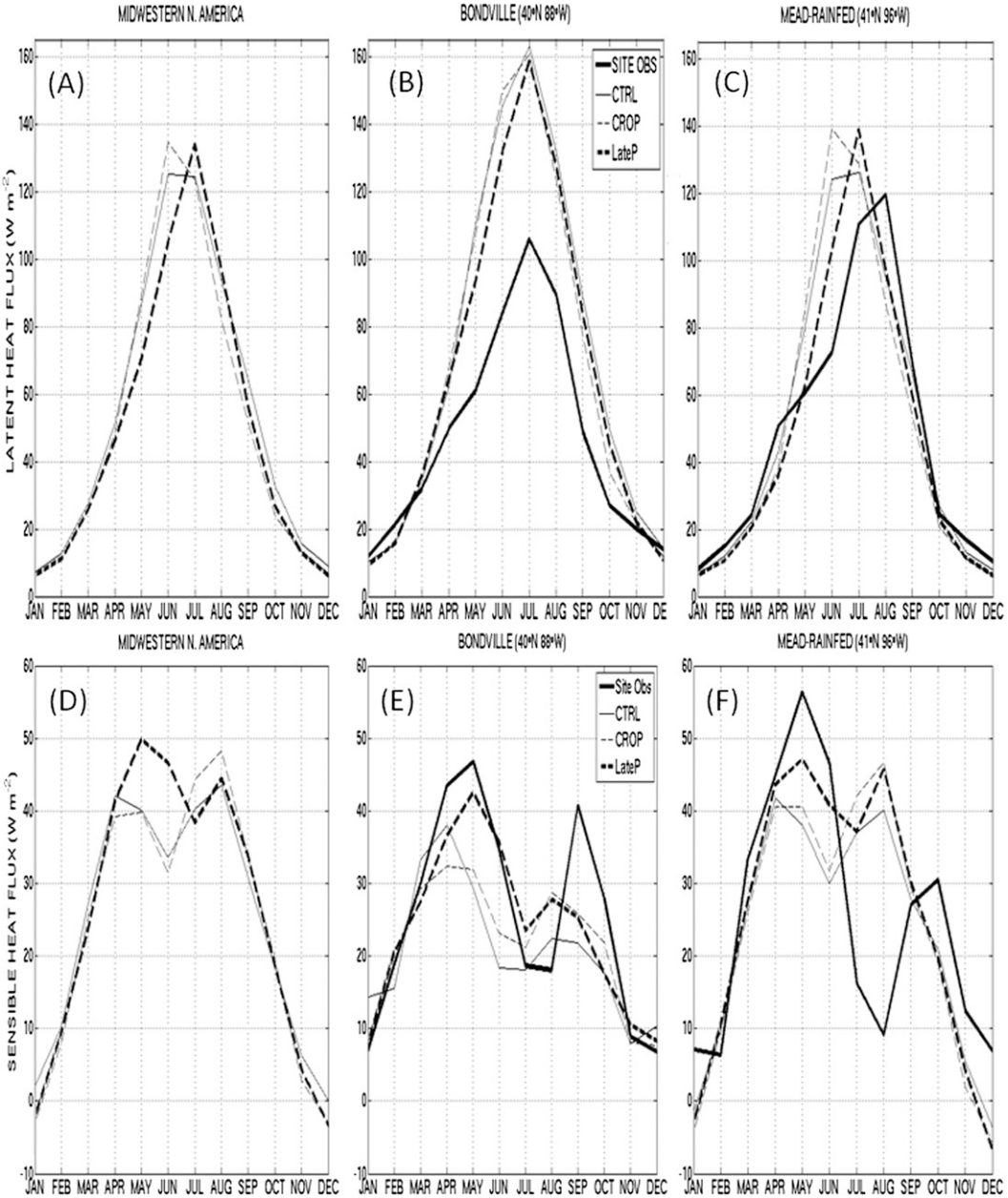

FIG. 3. Twenty-year-average monthly simulated turbulent heat fluxes: (a)–(c) latent and (d)–(f) sensible heat fluxes in midwestern North America, Bondville, and Mead, respectively. The site observations used for comparison are not 20-yr averages (see section 2c).

May and June and peaks one month early (July). At both sites the model overestimates L at least in May, June, and July.

Consistent with these patterns in L (earlier peak in CROP, later peak in LateP), CROP shows a later decline in P and LateP shows an earlier decline in P in midwestern North America (Fig. 4). The LateP June–August P compares very favorably to the observations but April and May degrade relative to the CTRL.

Simulated versus observed P in Bondville and Mead (not shown) generally agree with the regional result. In Mead, the site observations display a May–August double peak not captured by the model but also not shown in the gridded data (Willmott and Matsuura 2000). The double peak may be particular to the period of data collection in Mead. For example, climatological P data from Madison, Wisconsin, include a June–August double peak in some 30-yr climatologies (1951–80,

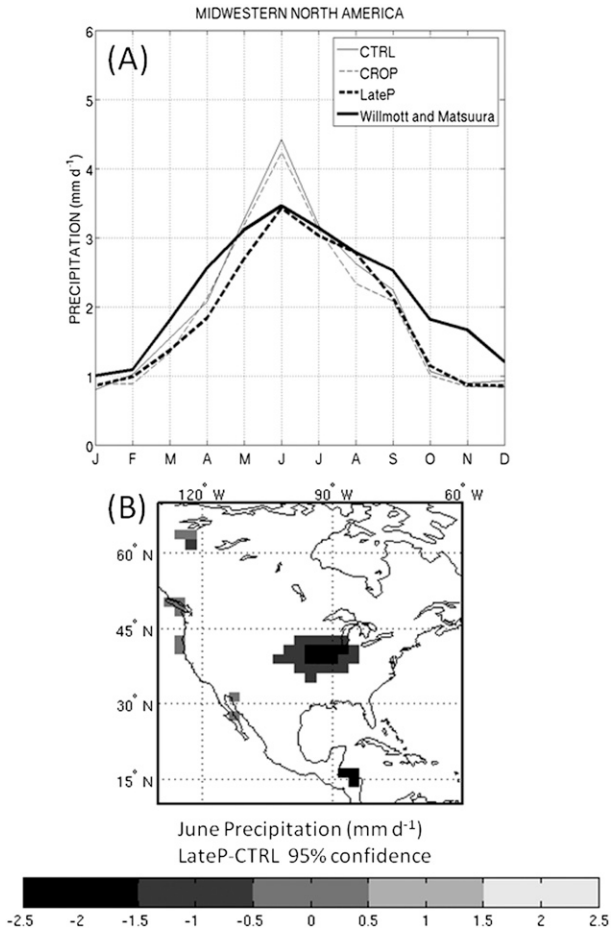

FIG. 4. Twenty-year-average monthly precipitation (a) simulated vs observed (Willmott and Matsuura 2000) in Midwestern North America and (b) difference (LateP minus CTRL simulations) in June in North America. Only statistically significant grid cells are shown (Student's t test, 95% confidence level).

1961–90, and 1971–2000), a June–September double peak in 1921–50, and not at all in others (1931–60 and 1941–70) (data available online at http://www.aos.wisc.edu/~sco/stations/msn/msn-normals.html).

The model output and the site observations do include double peaks in the sensible heat flux (H) (Figs. 3d–f). The model simulates the magnitude of the early peak closer to the observations at both sites (LateP performs best), while underestimating the later peak in Bondville and overestimating it in Mead. LateP simulates the timing of the early peak correctly at both sites, while CROP and CTRL tend to be a month early. The model simulates the second peak one and two months early in Bondville and Mead, respectively.

All three simulations overestimate summer T_{2m} in midwestern North America by 4–5 K (Willmott and Matsuura 2000) due to a bias in the coupled model. A simulation similar to our CTRL, with observed instead of climatological SSTs, simulates a 2–6 K summer bias in midwestern North America (R. Neale 2011, personal communication). The July peak and reduced June to July warming rate simulated in LateP matches in pattern the observations best. However, LateP overestimates spring T_{2m} more than the other simulations (Fig. 5a). Increases in spring and summer albedo (Table 2) and the associated potential for cooling relative to the CTRL may moderate, but apparently do not reverse, the added warming due to reduced L.

In June CROP simulates surface cooling northwest of the U. S. Midwest and little change or drying of 700-hPa specific humidity (q) in the Midwest due to minor changes in the advection of q (Fig. 5c). LateP simulates large surface warming over the managed crop region, still with little change in 700-hPa q over the Midwest (Fig. 5d). Farther northwest conditions appear moister, but the advection of q occurs from areas with little change or drying q.

The annual cycles of net ecosystem exchange (NEE) in Bondville and Mead show striking improvement in CROP and LateP relative to the CTRL (Fig. 6), more than any biogeophysical variable discussed in previous paragraphs. CROP peaks a month early, while LateP and the site observations peak in July. Using the simulated NEE, we diagnose monthly mean anomalies from the annual mean CO_2 concentration at five GLOBALVIEW monitoring stations. At all stations CROP and LateP show increased amplitude of the annual cycle relative to the CTRL, in better agreement with the observations (Fig. 7).

4. Discussion and conclusions

Traditionally, earth system model developers have represented managed vegetation as unmanaged grass because the availability of global-scale land management datasets and parameterizations for crop type, planting, harvesting, tillage, fertilization, and irrigation has lagged behind simple vegetation mapping. This is beginning to change, and we present changes and potential improvements in model simulations resulting from the replacement of unmanaged crop with corn, soybean, and temperate cereals in the coupled CAM4–CLM4CN.

From the simulations performed here, we reject the null hypothesis that we would not affect the CAM4 climate simulation by replacing the CLM4CN unmanaged crop with managed corn, soybean, and temperate cereals. For example, the coupled model simulates changes in North American temperature and precipitation due to changes in the turbulent heat fluxes and, in turn, the modified LAI. Furthermore, we find strong sensitivity of

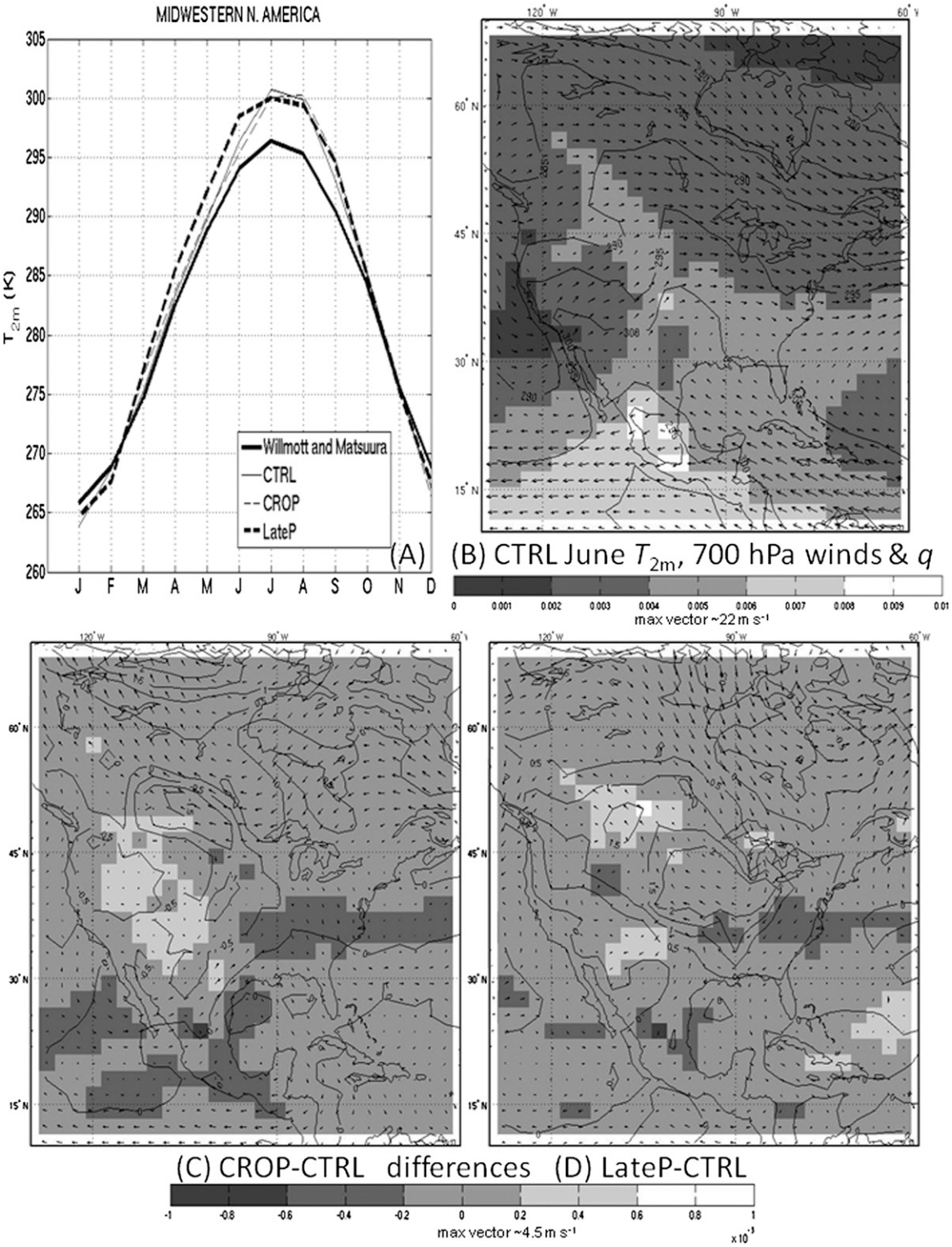

FIG. 5. Twenty-year-average monthly 2-m temperature (a) simulated vs observed (Willmott and Matsuura 2000) in Midwestern North America, (b) simulated in the CTRL in June in North America (isotherms range from 280 to 300 K), (c) difference for the CROP minus CTRL simulations in June in North America, and (d) the same but for LateP minus CTRL. (b)–(d) Also shown are the 700-hPa winds in vector form and the 700-hPa specific humidity (q) in grayscale, to assess moisture advection above the boundary layer.

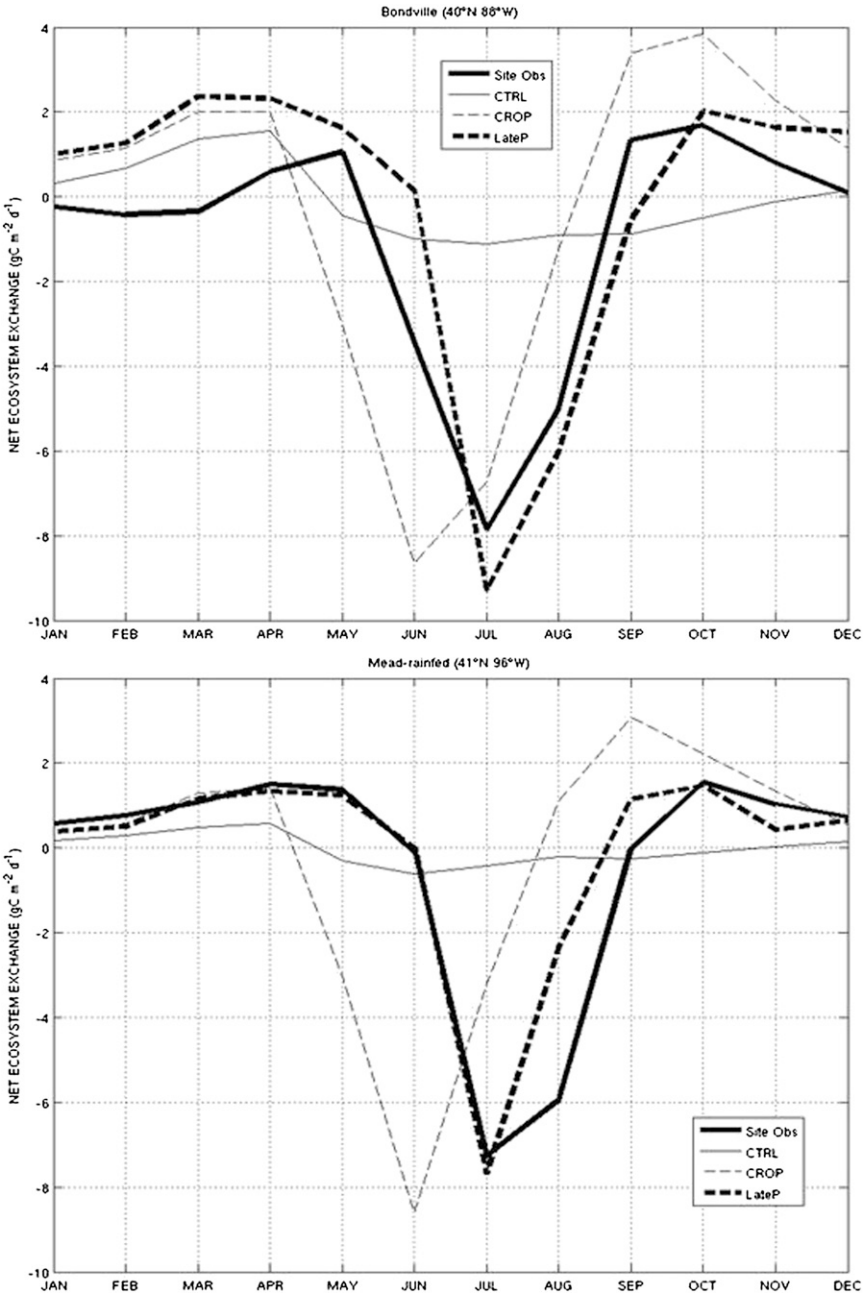

FIG. 6. Twenty-year-average monthly simulated net ecosystem exchange (NEE) in (a) Bondville and (b) Mead. The site observations used for comparison are not 20-yr averages (see section 2c).

midwestern North American simulated temperature and precipitation on the specific timing of crop greening. This result is in agreement with the results of Lu et al. (2001), who found strong seasonal climate–phenology interactions in the central United States.

In the CROP and CTRL simulations, midwestern crops begin to green in May. Both simulations peak in June–July, but CROP with appreciably higher LAI than in the CTRL (Figs. 2d–f). Likely because of the similar timing, CROP and CTRL display small differences in the atmospheric simulation despite the CROP higher summer and lower winter LAI. In contrast, crops in the LateP simulation begin to green in late June and peak in August, similar to the simulation for western Wisconsin

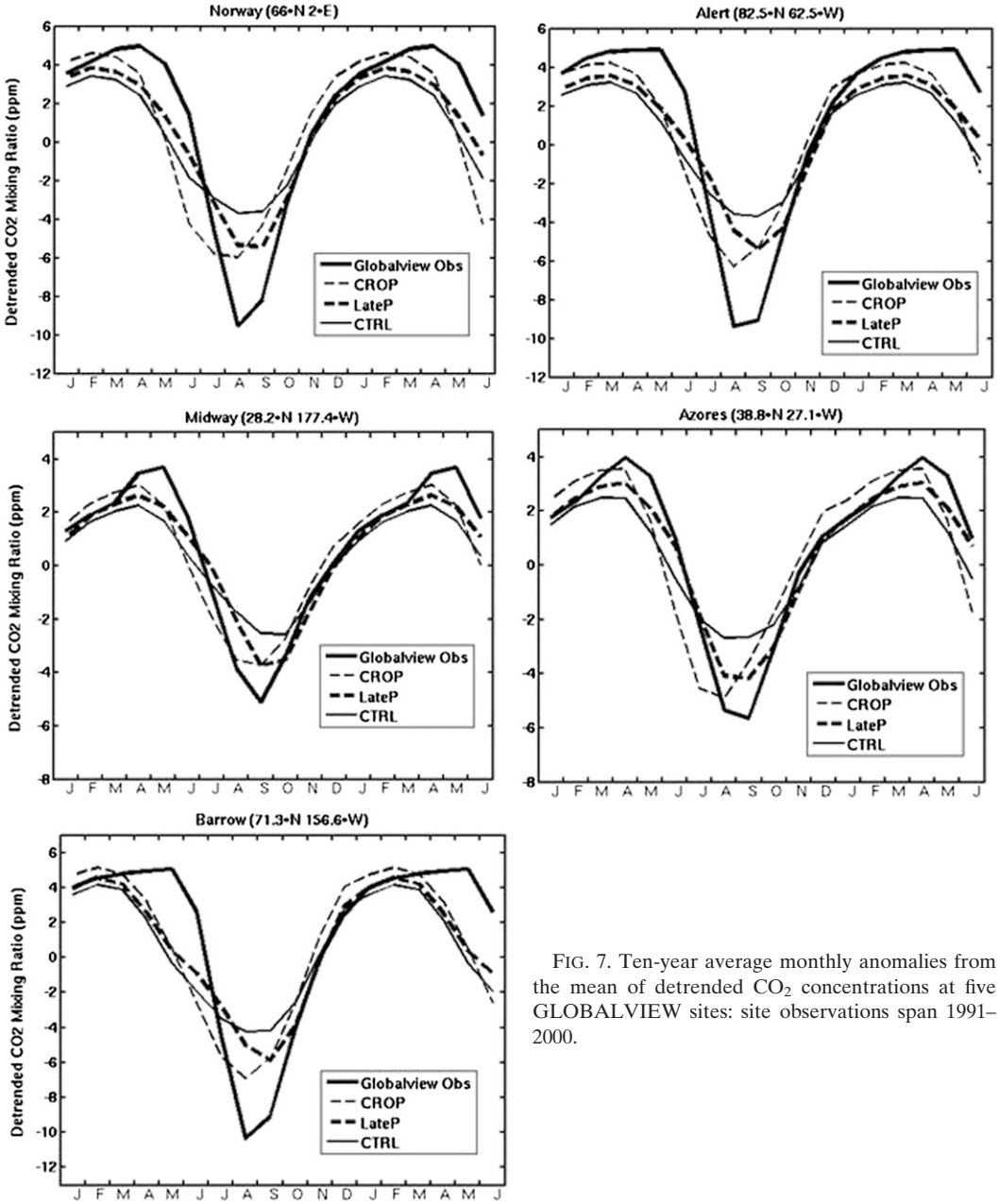

FIG. 7. Ten-year average monthly anomalies from the mean of detrended CO_2 concentrations at five GLOBALVIEW sites: site observations span 1991–2000.

in Twine et al. (2004). Delayed greening leads to reduced May–June latent heat flux, increased sensible heat flux, increased 2-m temperature, and reduced precipitation. Relative to the CROP and CTRL simulations, LateP simulates June precipitation closer to the observed (Willmott and Matsuura 2000). In other months, LateP precipitation differs less from CROP and the CTRL and does not always improve relative to the observations.

Extensive research on land–atmosphere interactions identifies midwestern North America as sensitive to changes in land surface properties (e.g., Oleson et al. 2004; Bonan 1997). In a thorough review, Raddatz (2007) summarized the observational and modeling literature and concluded that agriculture affects weather and climate on small to large spatial scales. Adegoke et al. (2007) summarized satellite-based observational work that correlates the timing and intensity of cloud development in the central United States to both synoptic flow and land surface characteristics. Raddatz and Cummine (2003) concluded that interactive crop phenology is crucial in land surface models for the correct

simulation of the latent heat flux and, therefore, thermodynamic properties of the atmospheric boundary layer over large agricultural regions, such as midwestern North America.

In a modeling study, Raddatz (1998) suggested that conversion of the Canadian Prairies from perennial grasses to annual field crops has decreased thunderstorm frequency early and late in the growing season and increased it in the height of the growing season. Raddatz (1999) suggested that the same conversion has warmed the daily maximum temperature early and late and cooled it in the height of the growing season. Our LateP springtime and September warming relative to the CTRL agrees with Raddatz (1999). Similarly our LateP May–June reduction of precipitation relative to the CTRL agrees with Raddatz (1998). The Raddatz modeling studies did not account for two-way land–atmosphere feedbacks. Our simulations do so and indicate a net loss of soil moisture with managed crops owing to generally reduced precipitation minus evaporation, especially at the peak of the growing season. To put our LateP results in the context of extreme drought, we mention the simulations of Cook et al. (2009) that captured the warmer and drier conditions of the dust bowl years in midwestern North America when removing the crops and accounting for the associated dust loading in the atmosphere and the drought inducing SSTs of the 1920s.

Beljaars et al. (1996) found that precipitation in the European Centre for Medium-Range Weather Forecasts model is simulated better when accounting for interactive soil moisture and when soils start the summer season with sufficient soil moisture. In a study based on observations in the Canadian Prairies, Hanesiak et al. (2009) showed that areas with wetter soils tend to experience severe summer convective weather more frequently than areas with drier soils. In a meticulous investigation of the effects of initial soil moisture anomalies on subsequent precipitation over North America using the coupled CAM3–CLM3, Kim and Wang (2007) found that spring soil moisture anomalies affected precipitation in summer, when convection is more prevalent, more than in spring and that the precipitation increased as they increased initial soil moisture. They also found that wet spring anomalies had a smaller effect, in magnitude and persistence, than dry spring anomalies. Similarly, Tsvetsinskaya et al. (2001b) found a greater effect from the interactive crop in drought years. Kim and Wang found that dry soil moisture anomalies suppressed evaporative cooling, increased surface temperature, and decreased sea level pressure. These changes weakened the westerlies and shifted them northward. Moisture divergence occurred over the Great Plains, while convergence and the precipitation moved northward. Qualitatively these conclusions applied in reverse for wet anomalies.

Our results are in qualitative agreement with the results of Kim and Wang (2007). Additional analysis of our results shows 700-hPa wind anomalies that reduce the westerlies north of 45°N in CROP and south of 45°N in LateP (Figs. 5c,d). CROP simulates slightly reduced sea level pressure over the southeastern United States and slightly increased over the western United States (Fig. 8). Slight divergence of 850-hPa winds in a band near 40°N increases omega, that is, subsidence at 500 hPa. These small changes result in a small decrease of June precipitation over the U. S. Midwest. LateP simulates a decrease in sea level pressure in the northern United States and develops an anticyclonic anomaly in 850 winds in the U. S. Midwest due to the warming. These changes intensify the southerly flow from the Gulf of Mexico mainly in the northern United States and central and western Canada, causing divergence south and east of these areas. Omega increases in large parts of the central United States (areas of divergence) and decreases north and west of there in central and western Canada. Increased subsidence coincides with the large reduction in precipitation over parts of midwestern North America.

Lu et al. (2001), Tsvetsinskaya et al. (2001b), and Kim and Wang (2007) agree that the land surface influence on sensible and latent heat fluxes and climate increases when local to regional atmospheric processes dominate over global phenomena. In midwestern North America this is true in summer when the jet stream weakens and local convective processes dominate over the large-scale circulation (Allard and Carleton 2010).

We have not accounted for irrigation in the present study. Irrigation in areas surrounding the Mead site (rainfed locally) may partly explain Mead's lower sensible heat flux in August relative to the model and compared to Bondville. No irrigation in the model may explain, in part, why we overestimate midwestern North American temperatures in summer. Sacks et al. (2009) found ~1 K cooling and almost a 1 mm d^{-1} increase in summer precipitation in the central United States when implementing realistic but prescribed irrigation rates in CAM3–CLM3 simulations. Would irrigation cancel the June bias reduction simulated in LateP by CAM4–CLM4? Interactive irrigation (not tested, yet, with this crop model) would not irrigate the crops until after leaf emergence, so the springtime reduction in latent heat flux and precipitation could persist.

The improved annual cycle in crop LAI simulated in the CROP and LateP simulations leads to a better simulated annual cycle of NEE in midwestern North America. From the increased amplitude in the annual

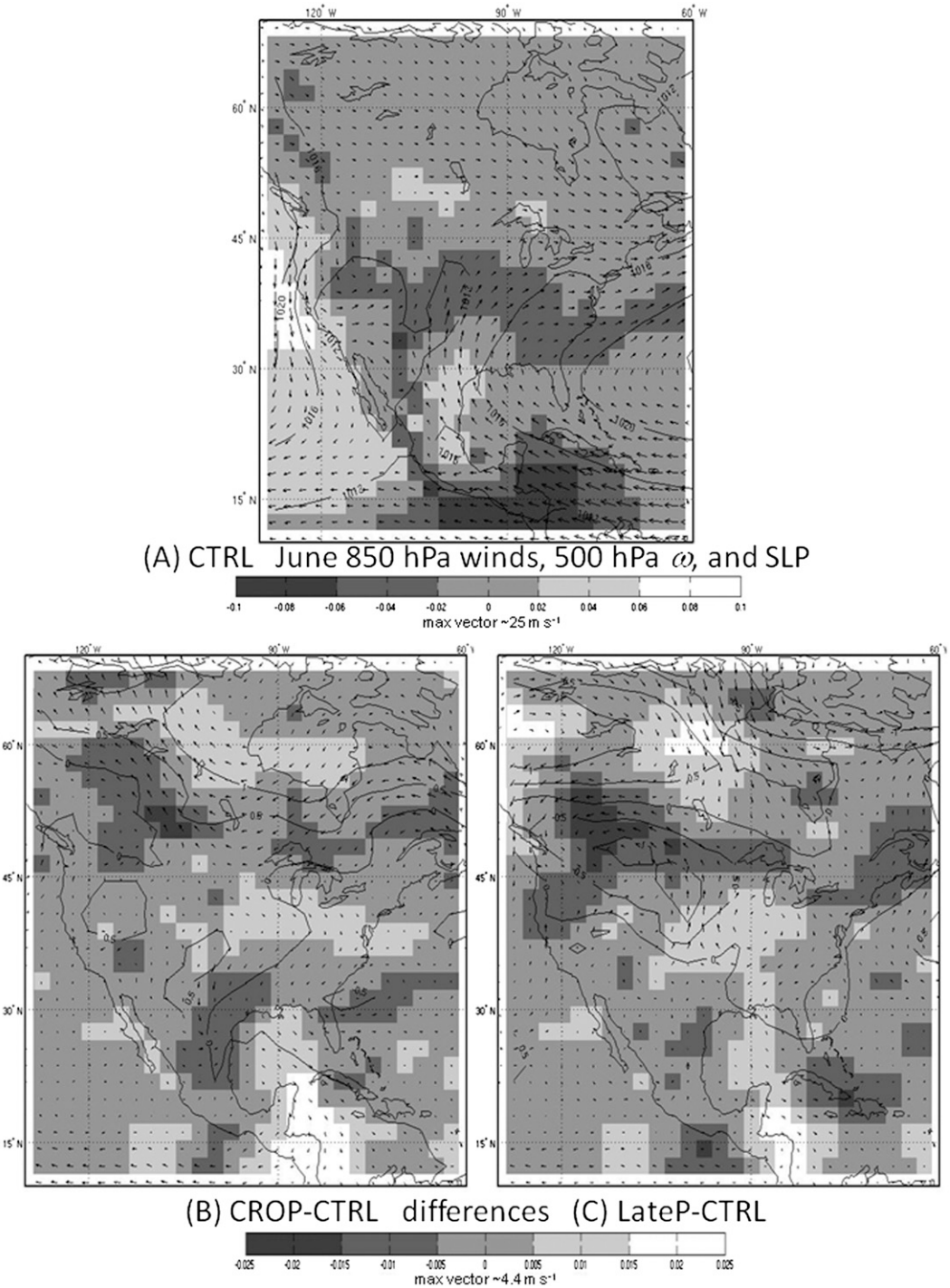

FIG. 8. Twenty-year-average monthly sea level pressure (SLP; isobars range from 1012 to 1020 hPa), 500-hPa vertical velocity (ω, in grayscale), and 850-hPa winds (vectors) (a) simulated in the CTRL in June in North America, (b) difference for the CROP minus CTRL simulations, and (c) the same but for LateP minus CTRL. The 850-hPa winds represent circulations near the surface.

cycle of the net ecosystem exchange, we diagnose a better annual cycle in CO_2 concentration anomalies at various sites around the world. Corbin et al. (2010) documented analogous improvements in CO_2 concentrations simulated in a regional coupled land–atmosphere model. Such refinements have promising implications for the simulation of prognostic atmospheric CO_2 when operating the fully coupled system (K. Lindsay 2012, unpublished manuscript).

In this study we have not controlled for the changes in plant functional type parameters that distinguish the managed from the unmanaged crops. We assume that the effects seen here originate primarily from LAI changes. More subtle effects from changing other pft parameters may be evaluated in a separate study.

These results justify the modeling community's continued attempts to improve the representation of crops in land surface models. The LateP simulation often behaves better than CROP relative to observations, but the growing season appears longer than the observed in both simulations. A CROP simulation driven with meteorological data (i.e., without the warm bias in midwestern North America) still overestimates the growing season length (not shown), suggesting a bias in our crop phenology calculations. We propose continued development in the representation of crops before adopting LateP as an improvement. At this early stage we mainly wish to emphasize the high sensitivity displayed by our atmospheric model to differences in the time of crop greening.

Agro-IBIS now includes some bioenergy cropping systems such as Miscanthus (VanLoocke et al. 2010). Updated versions of the CLM may include additional crops of societal significance, such as Miscanthus and rice, and additional forms of land management, for example, irrigation, fertilization, and double cropping to improve the realism of our simulations and to investigate crop sensitivity to nutrient and water limitations. Crop model applications may also include investigations on environmental degradation and protection (e.g., soil quality, fertilizer as pollutant, and societal encroachment into wilderness areas). Introducing human dimensions in models like the CESM will likely lead to the evolution of a new generation of models consisting of Integrated Assessment Models (Füssel 2010) coupled to earth system models. Such immediate to long term advances have the potential of improving fully coupled simulations with the CESM, while assisting human societies to answer pressing questions about food, energy, and water resources, as well as questions regarding climate change mitigation and adaptation.

Acknowledgments. Computing resources were provided by the Climate Simulation Laboratory at the National Center for Atmospheric Research (NCAR) Computational and Information Systems Laboratory (CISL). NCAR is sponsored by the National Science Foundation (NSF). CISL is sponsored by the NSF and other agencies. We thank C. Nevison for sharing scripts to extrapolate site-specific annual cycles of CO_2 concentration anomalies from simulated NEE. We thank three anonymous reviewers and X. Zeng for very helpful comments on the original manuscript. AJ was supported by the DOE under Contract DE-AC02-05CH11231.

APPENDIX

Technical Description of CLM4CN Crop

The following sections describe the CLM4CN crop model in detail. Very similar text (Levis and Sacks 2011) is posted together with other model documentation on the CLM page of the Community Earth System Model Web site (Available online at http://www.cesm.ucar.edu/models/cesm1.0/clm/index.shtml).

a. Crop plant functional types

The CLM default list of plant functional types (pfts) includes an unmanaged crop (Table 2.1, Oleson et al. 2010) treated as an unmanaged C3 grass. The unmanaged crop has gridcell coverage assigned from satellite data, as do all natural pfts when CLM4CNDV (dynamic vegetation) (Castillo et al. 2012) is not active.

The new crop pfts used in CLM4CNcrop get gridcell coverage from the present-day crop dataset of Ramankutty and Foley (1998). We assign these managed crops in the proportions given by Ramankutty and Foley without exceeding the area previously assigned to the unmanaged crop. The unmanaged crop continues to occupy any of its original area that remains and continues to be handled just by the CN part of CLM4CNcrop. The managed crop types (corn, soybean, and temperate cereals) were chosen based on the availability of corresponding algorithms in Agro-IBIS. Temperate cereals include wheat, barley, and rye here. We treat all temperate cereals as summer crops (like spring wheat, for example) at this time. We may introduce winter cereals (such as winter wheat) in a future version of the model.

To allow crops to coexist with natural vegetation in a grid cell and be treated by separate models (i.e., CNcrop versus CNDV), we separate the vegetated land unit into unmanaged and managed land units. Pfts in the unmanaged land unit share one soil column and compete for water (default CLM4 setting). Pfts in the managed land unit do not share soil columns to allow for different land management practices for different crops.

b. Phenology

CLM4CN includes evergreen, seasonally deciduous (responding to changes in day length), and stress deciduous (responding to changes in temperature and/or soil moisture) phenology algorithms. In CLM4CNcrop we have added the Agro-IBIS crop phenology algorithm, consisting of three distinct phases.

Phase 1 starts at planting and ends with leaf emergence, phase 2 continues from leaf emergence to the beginning of grain fill, and phase 3 starts from the beginning of grain fill and ends with physiological maturity and harvest.

1) Planting

Corn and temperate cereals must meet the following requirements between 1 April and 14 June for planting in the Northern Hemisphere (NH):

$$\begin{aligned} T_{10\mathrm{d}} &> T_p \\ T_{10\mathrm{d}}^{\min} &> T_p^{\min} \\ \mathrm{GDD}_8 &\geq \mathrm{GDD}_{\min}, \end{aligned} \tag{A1}$$

where $T_{10\mathrm{d}}$ is the 10-day running mean of $T_{2\mathrm{m}}$, (the simulated 2-m air temperature at every model time step), and $T_{10\mathrm{d}}^{\min}$ is the 10-day running mean of $T_{2\mathrm{m}}^{\min}$ (the daily minimum of $T_{2\mathrm{m}}$). The T_p and $T_p^{\min}$ are crop-specific coldest planting temperatures (Table A1), GDD_8 is the 20-yr running mean growing degree days (units are degree days or °days) tracked from April through September (NH) base 8°C with maximum daily increments of 30°days [see Eq. (A3)], and $\mathrm{GDD}_{\min}$ is the minimum growing degree-day requirement (Table A1). Soy must meet the same requirements but between 1 May and 14 June for planting. If the requirements in Eq. (A1) are not met by 14 June, then corn, soybean, and temperate cereals are still planted on 15 June as long as $\mathrm{GDD}_8 > 0$. In the Southern Hemisphere (SH) the NH requirements apply 6 months later.

GDD_8 does not change as quickly as $T_{10\mathrm{d}}$ and $T_{2\mathrm{d}}^{\min}$, so it determines whether the crop can be planted in a grid cell, while the two faster-changing variables determine when the crop may be planted.

At planting each crop is assigned 1 g leaf C m^{-2} pft column area to be transferred to the leaves upon leaf emergence. An equivalent amount of seed leaf nitrogen is assigned given the pft carbon (C) to nitrogen (N) ratio for leaves ($\mathrm{CN}_{\mathrm{leaf}}$). (This differs from Agro-IBIS, which uses a seed leaf area index instead of seed carbon.)

At planting, the model updates the average growing degree days necessary for the crop to reach vegetative and physiological maturity, $\mathrm{GDD}_{\mathrm{mat}}$, according to the following Agro-IBIS rules:

$$\begin{aligned} \mathrm{GDD}_{\mathrm{mat}}^{\mathrm{corn}} &= 0.85\mathrm{GDD}_8 \quad \text{and} \\ 950 < \mathrm{GDD}_{\mathrm{mat}}^{\mathrm{corn}} &< 1850\text{°days} \\ \mathrm{GDD}_{\mathrm{mat}}^{\mathrm{temp.cereals}} &= \mathrm{GDD}_0 \quad \text{and} \\ \mathrm{GDD}_{\mathrm{mat}}^{\mathrm{temp.cereals}} &< 1700\text{°days} \\ \mathrm{GDD}_{\mathrm{mat}}^{\mathrm{soy}} &= \mathrm{GDD}_{10} \quad \text{and} \\ \mathrm{GDD}_{\mathrm{mat}}^{\mathrm{soy}} &< 1700\text{°days}, \end{aligned} \tag{A2}$$

where GDD_{10} is the 20-yr running mean growing degree days tracked from April through September (NH) base 10°C with maximum daily increments of 30°days. Equation (A3) shows how we calculate GDD_0, GDD_8, and GDD_{10}:

$$\begin{aligned} \mathrm{GDD}_0 &= \mathrm{GDD}_0 + T_{2\mathrm{m}} - T_f \quad \text{where} \\ 0 &\leq T_{2\mathrm{m}} - T_f \leq 26\text{°days}, \\ \mathrm{GDD}_8 &= \mathrm{GDD}_8 + T_{2\mathrm{m}} - T_f - 8 \quad \text{where} \\ 0 &\leq T_{2\mathrm{m}} - T_f - 8 \leq 30\text{°days}, \\ \mathrm{GDD}_{10} &= \mathrm{GDD}_{10} + T_{2\mathrm{m}} - T_f - 10 \quad \text{where} \\ 0 &\leq T_{2\mathrm{m}} - T_f - 10 \leq 30\text{°days}, \end{aligned} \tag{A3}$$

where, if $T_{2\mathrm{m}} - T_f$ takes on values outside the above ranges, it equals the minimum or maximum value in the range. Also T_f equals 273.15 K, $T_{2\mathrm{m}}$ has units of K, and GDD has units of °days.

2) Leaf emergence

According to Agro-IBIS, leaves may emerge when the growing degree days of soil temperature to 0.05-m depth tracked since planting ($\mathrm{GDD}_{T_{\mathrm{soi}}}$) reaches 3% to 5% of $\mathrm{GDD}_{\mathrm{mat}}$ (Table A1). $\mathrm{GDD}_{T_{\mathrm{soi}}}$ is base 8°, 0°, and 10°C for corn, soybean, and temperate cereals. Leaf onset, as defined in the CN part of the model, occurs in the first time step of phase 2, at which moment all seed C is transferred to leaf C. Subsequently, the leaf area index generally increases and reaches a maximum value during phase 2.

3) Grain fill

Phase 3 begins in a similar way to phase 2. A variable tracked since planting like $\mathrm{GDD}_{T_{\mathrm{soi}}}$ but for 2-m air temperature, $\mathrm{GDD}_{T_{2\mathrm{m}}}$, must reach a heat unit threshold, h, from 40% to 70% of $\mathrm{GDD}_{\mathrm{mat}}$ (Table A1). For corn the percentage itself is an empirical function of $\mathrm{GDD}_{\mathrm{mat}}$ (not shown). In phase 3 the leaf area index begins to decline in response to a background litterfall

TABLE A1. Crop pfts in CLM4CNcrop and their parameters relating to phenology and morphology. Numbers in the first column correspond to the list of pfts in Table 2.1 of Oleson et al. (2010). Note that T_p and $T_p^{\min}$ are coldest planting temperatures but for winter cereals $T_p^{\min}$ is a warmest planting temperature. $\mathrm{GDD_{min}}$ is the lowest (for planting) 20-yr running mean growing degree days base 0°C (winter cereals) or 8 (other crops) tracked from April to September (NH). $\mathrm{GDD_{mat}}$ is a crop's 20-yr running mean growing degree days needed for vegetative and physiological maturity. Harvest occurs at 100% $\mathrm{GDD_{mat}}$ or when the days past planting reach the number in the 10th column. Crop growing season phases are described in the text. Here $z_{top}^{\max}$ is the maximum top-of-canopy height of a crop, SLA is specific leaf area, and leaf orientation index, χ_L, equals −1 for vertical, 0 for random, and 1 for horizontal leaf orientation.

Number and pft corresponding or added to CLM list of pfts	Phenological type	T_p (K)	$T_p^{\min}$ (K)	$\mathrm{GDD_{min}}$ (°days)	$\mathrm{GDD_{mat}}$ (°days)	Phase 2 (%$\mathrm{GDD_{mat}}$)	Phase 3 (%$\mathrm{GDD_{mat}}$)	Harvest (days Past planting)	$z_{\mathrm{top}}^{\max}$ (m)	SLA ($\mathrm{m^2}$ leaf $\mathrm{g^{-1}}$ C)	χ_L index
15 C_3 unmanaged crop	Stress Deciduous									0.03	−0.30
16 C_3 irrigated crop	Stress Deciduous									0.03	−0.30
17 Corn (also referred to as Maize)	Crop/Managed	283.15	279.15	50	950–1850	3	55–65	≤165	2.50	0.05	−0.50
18 Temperate cereals	Crop/Managed	280.15	272.15	50	≤1700	5	60	≤150	1.20	0.07	0.65
19 Winter cereals (place holder)	Crop/Managed		278.15	50	1900	5	40	≤265	1.20	0.07	0.65
20 Soybean	Crop/Managed	286.15	279.15	50	≤1700	3	70	≤150	0.75	0.07	−0.50

rate calculated as the inverse of leaf longevity for the pft.

4) HARVEST

Harvest is assumed to occur as soon as the crop reaches maturity. When $\mathrm{GDD}_{T_{2m}}$ reaches 100% of $\mathrm{GDD_{mat}}$ or the number of days past planting reaches a crop-specific maximum (Table A1), then the crop is harvested. Harvest occurs in one time step using the CN leaf offset algorithm. New variables track the flow of grain C and N to food and of live stem C and N to litter. Currently, food C and N are routed directly to litter using the CN distinction of labile, cellulose, and lignin fractions for leaves. The same fractions for leaves are used for the flow of live stem C and N to litter for corn, soybean, and temperate cereals. This is in contrast to the CLM4CN approach, which puts live stem C and N to dead steams first, rather than to litter.

c. *Allocation*

Allocation responds to the same phases as phenology (section b of this appendix). Simulated carbon assimilation begins every year upon leaf emergence in phase 2 and ends with harvest at the end of phase 3; therefore, so does the allocation of such carbon to the crop's leaf, live stem, fine root, and reproductive pools.

1) LEAF EMERGENCE TO GRAIN FILL

During phase 2, the allocation coefficients (fraction of available carbon) to each C pool are defined as

TABLE A2. Crop pfts in CLM4CNcrop and their parameters relating to allocation. Numbers in the first column correspond to the list of pfts in Table 2.1 of Oleson et al. (2010). Note that crop growing season phases and corresponding variables are described mostly in section c of the appendix.

Number and pft corresponding or added to CLM's list of pfts	Phase 2		Phases 2 and 3		Phase 3				
	a_{leaf}^{i} (fraction)	$L_{\max}$ ($\mathrm{m^2\ m^{-2}}$)	a_{froot}^{i} (fraction)	a_{froot}^{f} (fraction)	a_{leaf}^{f} (fraction)	$a_{\mathrm{livestem}}^{f}$ (fraction)	d_L (dimensionless)	$d_{\mathrm{alloc}}^{\mathrm{stem}}$ (dimensionless)	$d_{\mathrm{alloc}}^{\mathrm{leaf}}$ (dimensionless)
17 Corn (also referred to as maize)	0.800	5	0.400	0.050	0.000	0.000	1.05	2	5
18 Temperate cereals	0.750	7	0.300	0.000	0.000	0.050	1.05	1	3
19 Winter cereals (place holder)	0.425	7	0.300	0.000	0.000	0.050	1.05	1	3
20 Soybean	0.850	6	0.500	0.200	0.000	0.300	1.05	5	2

$$
\begin{aligned}
a_{\mathrm{repr}} &= 0,\\
a_{f\mathrm{root}} &= a^{i}_{f\mathrm{root}} - (a^{i}_{f\mathrm{root}} - a^{f}_{f\mathrm{root}})\frac{\mathrm{GDD}_{T_{2\mathrm{m}}}}{\mathrm{GDD}_{\mathrm{mat}}} \quad \text{where} \quad \frac{\mathrm{GDD}_{T_{2\mathrm{m}}}}{\mathrm{GDD}_{\mathrm{mat}}} \le 1,\\
a_{\mathrm{leaf}} &= (1 - a_{f\mathrm{root}})\frac{a^{i}_{\mathrm{leaf}}(e^{-b} - e^{[-b(\mathrm{GDD}_{T_{2\mathrm{m}}}/h)]})}{e^{-b} - 1} \quad \text{where} \quad b = 0.1,\\
a_{\mathrm{livestem}} &= 1 - a_{\mathrm{repr}} - a_{f\mathrm{root}} - a_{\mathrm{leaf}},
\end{aligned}
\tag{A4}
$$

where a^{i}_{leaf}, $a^{f}_{f\mathrm{root}}$, and $a^{i}_{f\mathrm{root}}$ are initial and final values of these coefficients (Table A2), and h is a heat unit threshold defined in appendix section b. At a crop-specific maximum leaf area index, $L_{\max}$ (Table A2), carbon allocation is directed exclusively to the fine roots.

2) Grain fill to harvest

The calculation of $a_{f\mathrm{root}}$ remains the same from phase 2 to phase 3. Other allocation coefficients change to

$$
\begin{aligned}
a_{\mathrm{leaf}} &= a^{i,3}_{\mathrm{leaf}} \quad \text{when} \quad a^{i,3}_{\mathrm{leaf}} \le a^{f}_{\mathrm{leaf}} \quad \text{else}\ldots,\\
a_{\mathrm{leaf}} &= a_{\mathrm{leaf}}\left(1 - \frac{\mathrm{GDD}_{T_{2\mathrm{m}}} - h}{\mathrm{GDD}_{\mathrm{mat}} d_L - h}\right)^{d^{\mathrm{leaf}}_{\mathrm{alloc}}} \ge a^{f}_{\mathrm{leaf}} \quad \text{where} \quad \frac{\mathrm{GDD}_{T_{2\mathrm{m}}} - h}{\mathrm{GDD}_{\mathrm{mat}} d_L - h} \le 1,\\
a_{\mathrm{livestem}} &= a^{i,3}_{\mathrm{livestem}} \quad \text{when} \quad a^{i,3}_{\mathrm{livestem}} \le a^{f}_{\mathrm{livestem}} \quad \text{else}\ldots,\\
a_{\mathrm{livestem}} &= a_{\mathrm{livestem}}\left(1 - \frac{\mathrm{GDD}_{T_{2\mathrm{m}}} - h}{\mathrm{GDD}_{\mathrm{mat}} d_L - h}\right)^{d^{\mathrm{stem}}_{\mathrm{alloc}}} \ge a^{f}_{\mathrm{livestem}} \quad \text{where} \quad \frac{\mathrm{GDD}_{T_{2\mathrm{m}}} - h}{\mathrm{GDD}_{\mathrm{mat}} d_L - h} \le 1,\\
a_{\mathrm{repr}} &= 1 - a_{f\mathrm{root}} - a_{\mathrm{livestem}} - a_{\mathrm{leaf}}
\end{aligned}
\tag{A5}
$$

where $a^{i,3}_{\mathrm{leaf}}$ and $a^{i,3}_{\mathrm{livestem}}$ (initial values) equal the last a_{leaf} and a_{livestem} calculated in phase 2, d_L, $d^{\mathrm{leaf}}_{\mathrm{alloc}}$ and $d^{\mathrm{stem}}_{\mathrm{alloc}}$ are leaf area index and leaf and stem allocation decline factors, and a^{f}_{leaf} and $a^{f}_{\mathrm{livestem}}$ are final values of these allocation coefficients (Table A2).

d. General comments

Carbon and nitrogen accounting now includes new pools and fluxes pertaining to live stems and reproductive tissues. For example, the calculations of growth respiration, above ground net primary production, litter fall, and displayed vegetation all now account for reproductive carbon.

We track allocation to reproductive C separately from the CN allocation to other carbon pools but within the CN framework. CN uses $a_{\mathrm{root}}/a_{\mathrm{leaf}}$ and $a_{\mathrm{livestem}}/a_{\mathrm{leaf}}$ to calculate C and N allometry and plant N demand. We also calculate $a_{\mathrm{repr}}/a_{\mathrm{leaf}}$ but merge the reproductive and live stem pools at this time instead of tracking them separately.

Stem area index (S) is equal to $0.1L$ for corn and $0.2L$ for other crops, as in Agro-IBIS, where L is the leaf area index. All live C and N pools go to 0 after crop harvest, but the S is kept at 0.25 to simulate a postharvest "stubble" on the ground.

Crop heights at the top and bottom of the canopy, z_{top} and z_{bot} (m), come from the Agro-IBIS formulation:

$$
\begin{aligned}
z_{\mathrm{top}} &= z^{\max}_{\mathrm{top}}\left(\frac{L}{L_{\max} - 1}\right)^{2} \ge 0.05, \quad \text{where} \quad \frac{L}{L_{\max} - 1} \le 1\\
z_{\mathrm{bot}} &= 0.02\mathrm{m}
\end{aligned}
\tag{A6}
$$

The CN part of the model keeps track of a term representing excess maintenance respiration that for perennial pfts or pfts with carbon storage may be extracted from later gross primary production (GPP). Annual crops do not have GPP or C storage after harvest, so at harvest we extract CO_2 directly from the atmosphere to return the excess respiration pool to zero.

An implementation of interactive fertilization is forthcoming (B. Drewniak 2011, personal communication) and interactive irrigation does not work for corn, soybean, and temperate cereals, yet. Therefore, we consider all pfts rainfed, and we disable the CLM4CN interactive nitrogen limitation for corn, soybean, and

temperate cereals. Instead, we prescribe the V_{cmax25} value (101) proposed for crops by Kattge et al. (2009) as used in carbon-only simulations with the CLM4 by Bonan et al. (2011).

In the list of plant physiological and other parameters used by CLM4CN, we started the managed crops with the existing values assigned to the unmanaged C3 crop. Then we changed the following parameters to distinguish corn, soybean, and temperate cereals from the unmanaged C3 crop and from each other:

- growth respiration coefficient from 0.30 to the Agro-IBIS value of 0.25;
- fraction of leaf N in the Rubisco enzyme from 0.1 to 0.2 g N Rubisco g^{-1} N leaf for temperate cereals to increase productivity (not chosen based on Agro-IBIS);
- fraction of current photosynthesis displayed as growth changed from 0.5 to 1 (not chosen based on Agro-IBIS)—this means that no photosynthesis goes to storage pools;
- CLM4CN values of the C to N ratio, CN, rather than values from Agro-IBIS—for reproductive C we used the value for live wood, CN_{lw}, equal to 50—and changed CN_{leaf_litter} to equal CN_{leaf}, so as to suppress retranslocation;
- CLM4CN curve for the effect of temperature on photosynthesis instead of crop-specific curves from Agro-IBIS;
- quantum efficiency at 25°C, α, from 0.06 to 0.04 μmol CO_2 μmol^{-1} photon for C4 crops (corn), using the CLM4CN C4 grass value;
- slope m of conductance-to-photosynthesis relationship from 9 to 4 for C4 crops as in Agro-IBIS;
- specific leaf areas, SLA, to the Agro-IBIS values (Table A1);
- leaf orientation, χ_L, to the Agro-IBIS values (Table A1); and
- soil moisture photosynthesis limitation factor, β_t, for soybeans multiplied as in Agro-IBIS by 1.25 for increased drought tolerance.

REFERENCES

Adegoke, J. O., R. Pielke, and A. M. Carleton, 2007: Observational and modeling studies of the impacts of agriculture-related land use change on planetary boundary layer processes in the central US. *Agric. For. Meteor.,* **142,** 203–215.

Allard, J., and A. M. Carleton, 2010: Mesoscale associations between Midwest land surface properties and convective cloud development in the warm season. *Phys. Geogr.,* **31,** 107–136.

Beljaars, A. C. M., P. Viterbo, M. J. Miller, and A. K. Betts, 1996: The anomalous rainfall over the United States during July 1993: Sensitivity to land surface parameterization and soil moisture anomalies. *Mon. Wea. Rev.,* **124,** 362–383.

Bonan, G. B., 1997: Effects of land use on the climate of the United States. *Climatic Change,* **37,** 449–486.

——, and Coauthors, 2011: Improving canopy processes in the Community Land Model (CLM4) using global flux fields empirically inferred from FLUXNET data. *J. Geophys. Res.,* **116,** G02014, doi:10.1029/2010JG001593.

Bondeau, A., and Coauthors, 2007: Modelling the role of agriculture for the 20th century global terrestrial carbon balance. *Global Change Biol.,* **13,** 679–706, doi:10.1111/j.1365-2486.2006.01305.x.

Castillo, C. K. G., S. Levis, and P. E. Thornton, 2012: Evaluation of the new CNDV option of the Community Land Model: Effects of dynamic vegetation and interactive nitrogen on CLM4 means and variability. *J. Climate,* **25,** 3702–3714.

Cook, B. I., R. L. Miller, and R. Seager, 2009: Amplification of the North American "Dust Bowl" drought through human-induced land degradation. *Proc. Natl. Acad. Sci. USA,* **106,** 4997–5001.

Corbin, K. D., A. S. Denning, E. Y. Lokupitiya, A. E. Schuh, N. L. Miles, K. J. Davis, S. Richardson, and I. T. Baker, 2010: Assessing the impact of crops on regional CO_2 fluxes and atmospheric concentrations. *Tellus,* **62B,** 521–532.

Donner, S. D., and C. J. Kucharik, 2003: Evaluating the impacts of land management and climate variability on crop production and nitrate export across the Upper Mississippi Basin. *Global Biogeochem. Cycles,* **17,** 1085, doi:10.1029/2001GB001808.

Flénet, F., J. R. Kiniry, J. E. Board, M. E. Westgate, and D. C. Reicosky, 1996: Row spacing effects on light extinction coefficients of corn, sorghum, soybean, and sunflower. *Agron. J.,* **88,** 185–190.

Foley, J. A., and Coauthors, 1996: An integrated biosphere model of land surface processes, terrestrial carbon balance, and vegetation dynamics. *Global Biogeochem. Cycles,* **10,** 603–628.

Füssel, H.-M., 2010: Modeling impacts and adaptation in global IAMs. *WIREs Climate Change,* **1,** 288–303.

Gent, P. R., and Coauthors, 2011: The Community Climate System Model, version 4. *J. Climate,* **24,** 4973–4991.

Gervois, S., P. Ciais, N. de Noblet-Ducoudré, N. Brisson, N. Vuichard, and N. Viovy, 2008: Carbon and water balance of European croplands throughout the 20th century. *Global Biogeochem. Cycles,* **22,** GB2022, doi:10.1029/2007GB003018.

Hanesiak, J., A. Tat, and R. L. Raddatz, 2009: Initial soil moisture as a predictor of subsequent severe summer weather in the cropped grassland of the Canadian Prairie provinces. *Int. J. Climatol.,* **29,** 899–909.

Hodges, T., D. Botner, C. Sakamoto, and J. H. Haug, 1987: Using the CERES-MAIZE model to estimate production for the United States corn belt. *Agric. For. Meteor.,* **40,** 293–303.

Jung, M., M. Reichstein, and A. Bondeau, 2009: Towards global empirical upscaling eddy covariance observations: Validation of a model tree ensemble approach using a biosphere model. *Biogeosci. Discuss.,* **6,** 5271–5304.

Kattge, J., W. Knorr, T. Raddatz, and C. Wirth, 2009: Quantifying photosynthetic capacity and its relationship to leaf nitrogen content for global-scale terrestrial biosphere models. *Global Change Biol.,* **15,** 976–991.

Kim, Y., and G. Wang, 2007: Impact of initial soil moisture anomalies on subsequent precipitation over North America in the coupled land–atmosphere model CAM3-CLM3. *J. Hydrometeor.,* **8,** 513–533.

Kluzek, E., cited 2011: CESM research tools: CLM4 in CESM1.0.3 user's guide documentation. [Available online at http://www.cesm.ucar.edu/models/cesm1.0/clm/index.shtml.]

Koster, R. D., and Coauthors, 2004: Regions of strong coupling between soil moisture and precipitation. *Science,* **305,** 1138–1140.

Kucharik, C. J., 2003: Evaluation of a process-based agroecosystem model (Agro-IBIS) across the U.S. corn belt: Simulations of the interannual variability in maize yield. *Earth Interact.,* **7.** [Available online at http://EarthInteractions.org.]

——, and K. R. Brye, 2003: Integrated BIosphere Simulator (IBIS) yield and nitrate loss predictions for Wisconsin maize receiving varied amounts of nitrogen fertilizer. *J. Environ. Qual.,* **32,** 247–268.

——, and T. E. Twine, 2007: Residue, respiration, and residuals: Evaluation of a dynamic agroecosystem model using eddy flux measurements and biometric data. *Agric. For. Meteor.,* **146,** 134–158.

——, J. A. Foley, C. Delire, V. A. Fisher, M. T. Coe, J. D. Lenters, C. Young-Molling, and N. Ramankutty, 2000: Testing the performance of a dynamic global ecosystem model: Water balance, carbon balance, and vegetation structure. *Global Biogeochem. Cycles,* **14,** 795–825.

Lawrence, D. M., K. W. Oleson, M. G. Flanner, C. G. Fletcher, P. J. Lawrence, S. Levis, S. C. Swenson, and G. B. Bonan, 2012: The CCSM4 land simulation, 1850–2005: Assessment of surface climate and new capabilities. *J. Climate,* **25,** 2240–2260.

Levis, S., 2010: Modeling vegetation and land use in models of the earth system. *WIREs Climate Change,* **1,** 840–856, doi:10.1002/wcc.83.

——, and W. J. Sacks, cited 2011: Technical descriptions of the interactive crop management (CLM4CNcrop) and interactive irrigation models in version 4 of the Community Land Model. [Available online at http://www.cesm.ucar.edu/models/cesm1.0/clm/index.shtml.]

——, P. Thornton, G. Bonan, and C. Kucharik, 2009: Modeling land use and land management with the Community Land Model. *iLeaps Newsletter,* No. 7, University of Helsinki, Helsinki, Finland, 10–12.

Lokupitiya, E., and Coauthors, 2009: Incorporation of crop phenology in Simple Biosphere Model (SiBcrop) to improve land-atmosphere carbon exchanges from croplands. *Biogeosciences,* **6,** 969–986.

Lu, L., R. A. Pielke Sr., G. E. Liston, W. J. Parton, D. Ojima, and M. Hartman, 2001: Implementation of a two-way interactive atmospheric and ecological model and its application to the central United States. *J. Climate,* **14,** 900–919.

Masarie, K. A., and P. P. Tans, 1995: Extension and integration of atmospheric carbon-dioxide data into a globally consistent measurement record. *J. Geophys. Res.,* **100D,** 11 593–11 610.

Mearns, L. O., T. Mavromatis, E. Tsvetsinskaya, C. Hays, and W. E. Easterling, 1999: Comparative responses of EPIC and CERES crop models to high and low spatial resolution climate change scenarios. *J. Geophys. Res.,* **104D,** 6623–6646.

Meyers, T. P., and S. E. Hollinger, 2004: An assessment of storage terms in the surface energy balance of maize and soybean. *Agric. For. Meteor.,* **125,** 105–115.

Oleson, K. W., G. B. Bonan, S. Levis, and M. Vertenstein, 2004: Effects of land use change on North American climate: Impact of surface datasets and model biogeophysics. *Climate Dyn.,* **23,** 117–132.

——, and Coauthors, 2010: Technical description of version 4.0 of the Community Land Model (CLM). NCAR Tech. Note NCAR/TN-478+STR, 257 pp.

Osborne, T. M., D. M. Lawrence, A. J. Challinor, J. M. Slingo, and T. R. Wheeler, 2007: Development and assessment of a coupled crop–climate model. *Global Change Biol.,* **13,** 169–183, doi:10.1111/j.1365-2486.2006.01274.x.

——, J. M. Slingo, D. M. Lawrence, and T. R. Wheeler, 2009: Examining the interaction of growing crops with local climate using a coupled crop–climate model. *J. Climate,* **22,** 1393–1411.

Pitman, A. J., and Coauthors, 2009: Uncertainties in climate responses to past land cover change: First results from the LUCID intercomparison study. *Geophys. Res. Lett.,* **36,** L14814, doi:10.1029/2009GL039076.

Raddatz, R. L., 1998: Anthropogenic vegetation transformation and the potential for deep convection on the Canadian prairies. *Can. J. Soil Sci.,* **78,** 657–666.

——, 1999: Anthropogenic vegetation transformation and maximum temperatures on the Canadian prairies. *CMOS Bull.,* **27,** 167–173.

——, 2007: Evidence for the influence of agriculture on weather and climate through the transformation and management of vegetation: Illustrated by examples from the Canadian prairies. *Agric. For. Meteor.,* **142,** 186–202.

——, and J. D. Cummine, 2003: Inter-annual variability of moisture flux from the prairie agro-ecosystem: Impact of crop phenology on the seasonal pattern of tornado days. *Bound.-Layer Meteor.,* **106,** 283–295.

Ramankutty, N., and J. A. Foley, 1998: Characterizing patterns of global land use: An analysis of global croplands data. *Global Biogeochem. Cycles,* **12,** 667–685.

Randerson, J. T., and Coauthors, 2009: Systematic assessment of terrestrial biogeochemistry in coupled climate–carbon models. *Global Change Biol.,* **15,** 2462–2484, doi:10.1111/j.1365-2486.2009.01912.x.

Sacks, W. J., B. I. Cook, N. Buenning, S. Levis, and J. H. Helkowski, 2009: Effects of global irrigation on the near-surface climate. *Climate Dyn.,* **33,** 159–175, doi:10.1007/s00382-008-0445-z.

Stehfest, E., M. Heistermann, J. A. Priess, D. S. Ojima, and J. Alcamo, 2007: Simulation of global crop production with the ecosystem model DayCent. *Ecol. Modell.,* **209,** 203–219.

Thenkabail, P. S., R. B. Smith, and E. De Pauw, 2000: Hyperspectral vegetation indices and their relationships with agricultural crop characteristics. *Remote Sens. Environ.,* **71,** 158–182.

Tsvetsinskaya, E. A., L. O. Mearns, and W. E. Easterling, 2001a: Investigating the effect of seasonal plant growth and development in three-dimensional atmospheric simulations. Part I: Simulation of surface fluxes over the growing season. *J. Climate,* **14,** 692–709.

——, ——, and ——, 2001b: Investigating the effect of seasonal plant growth and development in three-dimensional atmospheric simulations. Part II: Atmospheric response to crop growth and development. *J. Climate,* **14,** 711–729.

Twine, T. E., and C. J. Kucharik, 2008: Evaluating a terrestrial ecosystem model with satellite information of greenness. *J. Geophys. Res.,* **113,** G03027, doi:10.1029/2007JG000599.

——, ——, and J. A. Foley, 2004: Effects of land cover change on the energy and water balance of the Mississippi River basin. *J. Hydrometeor.,* **5,** 640–655.

VanLoocke, A., C. J. Bernacchi, and T. E. Twine, 2010: The impacts of Miscanthus x giganteus production on the Midwest

U.S. hydrologic cycle. *Global Change Biol. Bioenergy,* **2,** 180–191, doi:10.1111/j.1757-1707.2010.01053.x.

Verma, S. B., and Coauthors, 2005: Annual carbon dioxide exchange in irrigated and rainfed maize-based agroecosystems. *Agric. For. Meteor.,* **131,** 77–96.

Willmott, C. J., and K. Matsuura, cited 2000: Terrestrial air temperature and precipitation: Monthly and annual climatologies. [Available online at http://climate.geog.udel.edu/~climate.]

Wilson, K. B., P. J. Hanson, P. J. Mulholland, D. D. Baldocchi, and S. D. Wullschleger, 2001: A comparison of methods for determining forest evapotranspiration and its components: Sapflow, soil water budget, eddy covariance and catchment water balance. *Agric. For. Meteor.,* **106,** 153–168, doi:10.1016/S0168-1923(00)00199-4.

Xue, Y., M. J. Fennessy, and P. J. Sellers, 1996: Impact of vegetation properties on U.S. summer weather prediction. *J. Geophys. Res.,* **101D,** 7419–7430.

DISCLAIMER

This document was prepared as an account of work sponsored by the United States Government. While this document is believed to contain correct information, neither the United States Government nor any agency thereof, nor The Regents of the University of California, nor any of their employees, makes any warranty, express or implied, or assumes any legal responsibility for the accuracy, completeness, or usefulness of any information, apparatus, product, or process disclosed, or represents that its use would not infringe privately owned rights. Reference herein to any specific commercial product, process, or service by its trade name, trademark, manufacturer, or otherwise, does not necessarily constitute or imply its endorsement, recommendation, or favoring by the United States Government or any agency thereof, or The Regents of the University of California. The views and opinions of authors expressed herein do not necessarily state or reflect those of the United States Government or any agency thereof or The Regents of the University of California.

Ernest Orlando Lawrence Berkeley National Laboratory is an equal opportunity employer.